

Electron capture in collisions of protons with CO molecules in the keV region: The steric effectMineo Kimura,* Jian-ping Gu,[†] Gerhard Hirsch, and Robert J. Buenker[†]*Theoretische Chemie, Bergische Universität-Gesamthochschule Wuppertal, D-42097 Wuppertal, Germany*

P. C. Stancil

*Physics Division, Oak Ridge National Laboratory, Oak Ridge, Tennessee 37831-6372**and Department of Physics and Astronomy, University of Tennessee, Knoxville, Tennessee 37996-1200*

(Received 13 November 1998; revised manuscript received 3 February 1999; published 11 February 2000)

Electron capture resulting from collisions of H^+ ions with CO molecules has been investigated based on the molecular representation within the fully quantum-mechanical formalism below 10 keV/u. Three different molecular configurations have been considered for collision dynamics, i.e., (i) the proton approaches the center of mass of the CO molecule in the perpendicular configuration, (ii) the proton approaches the C atom in the collinear configuration, and (iii) the proton approaches the O atom in the collinear configuration. Electron-capture dynamics and corresponding capture cross sections depend very sensitively on the molecular configuration, thus revealing a strong steric effect. The capture cross section from the CO electronic ground state is about $1.3 \times 10^{-15} \text{ cm}^2$ at 10 keV/u, which is in good agreement with experimental findings. Differential cross sections (DCS's) for three molecular orientations have been examined both for elastic and electron-capture processes, and the DCS averaged over all the configurations was found to agree well with a measurement from 0.02° to 1° at 1.5 keV/u.

PACS number(s): 34.50.-s, 34.20.Mq, 34.70.+e

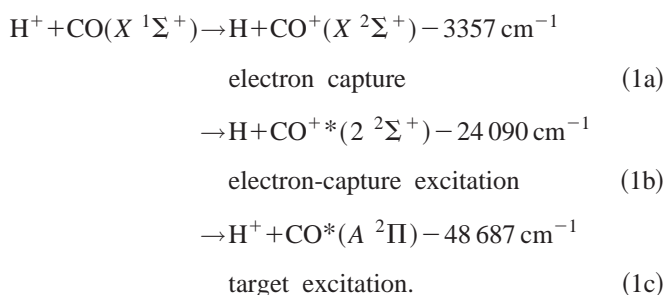
I. INTRODUCTION

Electron capture from a molecular target due to ion impact has been known to be extremely sensitive to the molecular orientation, i.e., the steric effect, particularly for low-energy reactive scattering, as implied by several theoretical studies [1,2]. Recently, there have been reported some experimental attempts to fix the molecular orientation during collisions by using the octapole magnet method and to carry out the experiment for various scattering processes [3,4]. For high-energy scattering above the keV-energy domain, the steric effect becomes somewhat less pronounced because the projectile passes through the interaction region very quickly, compared to that at lower energies, but it still plays an important role for understanding collision dynamics. Until recently, the orientation-averaged cross section is usually only considered.

However, in our series of investigations, we have shown that the orientation effect still persists even in low keV-collision energies for CH_4 [5] and C_2H_2 [6] targets. Depending upon the molecular orientation, electron-capture cross sections were found to differ by more than an order of magnitude at 1 keV/u. However, at small scattering angles less than a few degrees, the magnitude of the differential cross sections for different molecular orientations are comparable. Further, a strong interference oscillatory pattern in the differential cross section was found, which was also experimentally supported. These findings are significant both in terms

of fundamental atomic physics and in relation to their application in other fields.

In continuing this series of papers on molecular targets, we have carried out theoretical investigations for electron capture resulting from proton collisions with CO molecules for collision energies less than 10 keV, and have intended to examine more specifically the steric effect on capture dynamics. The process is important in various applications. Specifically, the process is important for modeling the interaction of the solar wind with comets [7]. Protons are the dominant species in the solar wind [8] while the coma is composed of about 15% CO [9]. Charge transfer with the cometary neutrals may explain the loss of solar wind protons observed at comet Halley [7]. The reverse reaction may also play a role in diffuse interstellar cloud chemistry. Also, the carbon monoxide (CO) molecule is important for various applications in fusion research, plasma chemistry, and medical physics for cancer research. Furthermore, the CO molecule is chosen in this study because it is expected to show an enhanced steric effect due to its heteronuclear structure, and hence can provide much detailed information on collision dynamics. The processes we are concerned with are



Because of the small energy defect, process (1a) is expected to dominate in the energy region considered, while processes (1b) and (1c) are weaker channels with the energy defect larger than 3 eV. Note that the energy defects in Eqs. (1a)–

*Permanent address: School of Medicine, Yamaguchi University, Ube, Yamaguchi 755, Japan.

[†]Present address: Institute for Theoretical Atomic and Molecular Physics, Harvard-Smithsonian Center for Astrophysics, 60 Garden Street, Cambridge, MA 02138.

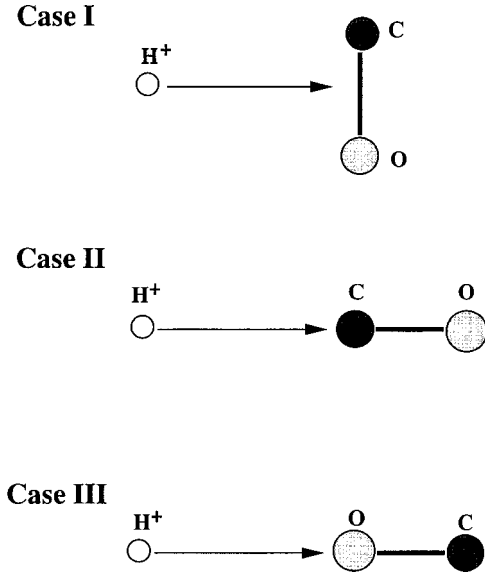


FIG. 1. Diagram of the molecular configurations for three cases.

(1c) are determined based on the assumption that the C-O distance is fixed at the equilibrium distance.

As for the orientation, we have considered three molecular configurations: (i) the H⁺ approaches the center of mass of CO (CO perpendicular to the incoming H⁺), (ii) H⁺ approaches the C atom, in which CO lies along the collision trajectory (collinear case), and (iii) the H⁺ approaches toward the O atom (also collinear case). The investigation of these three molecular orientations should give significant insight into the details of the steric effect for electron capture, and is expected to provide a general guideline for further experimental research.

Recently, related experimental work has been performed by several groups. There are numerous experimental studies on electron capture, but the following four studies are the most relevant to the current investigations. Browning and Gilbody [10] have investigated molecular fragmentation of CO by using proton impact in the energy region from 5 to 45 keV/u. Rudd *et al.* [11] have measured ionization and electron capture resulting from proton impact in the energy region between 5 and 150 keV/u. More recently, Shah and Gilbody [12] have measured electron-capture cross sections from the CO molecule in the energy region from 10 to 100 keV/u, and Gao *et al.* [13] have performed differential cross-section measurements for various molecular targets at 1.5 keV/u by H⁺- and He⁺-ion impacts. This last study is expected to serve as a stringent test for the present theoretical calculation, and to provide basic understanding of the collision dynamics.

II. THEORETICAL MODELS

A. Molecular states

The *ab initio* calculations are performed for three different cases (cases I–III) as shown in Fig. 1. That is to say that H⁺ approaches CO in three different configurations. In case I, H⁺ vertically approaches the mass center of CO along the

TABLE I. Number of reference configurations N_{ref} and number of roots N_{root} treated in each irreducible representation and the corresponding number of generated (N_{tot}) and selected (N_{sel}) symmetry-adapted functions for a threshold of 0.32×10^{-6} hartree at $R = 2.0a_0$. Note that R is the distance between H⁺ and the CO center of mass.

State	$N_{\text{ref}}/N_{\text{root}}$	N_{tot}	N_{sel}
Case I			
1 $^1A'$	63/4	4 017 024	177 744
1 $^1A''$	38/2	2 692 591	111 015
Case II			
1A_1	52/3	1 913 718	73 838
1B_1	33/2	1 264 946	75 195
Case III			
1A_1	46/3	1 648 651	97 443
1B_1	40/2	1 590 851	94 605

Z axis. CO is located along the Y axis. The only symmetry plane for the system is the YZ plane (C_s point group) and the electronic states are classified according to the two irreducible representations, A' and A'' , of the C_s point group. In this case the interactions are through radial couplings between A' states, the X component of the rotational couplings between A' states, and the Y and Z components of the rotational couplings between A' and A'' states. Other interactions are excluded due to symmetry constraints. In both cases II and III the H⁺ approaches CO collinearly. Transitions are driven by relevant radial and rotational couplings. CO lies along the collision trajectory. The H⁺ approaches toward the C atom in case II and toward the O atom in case III. In cases II and III the calculations are done in the C_{2v} subgroup (the highest Abelian subgroup) of the $C_{\infty v}$ point group. In all three cases, the origin of the scattering coordinates is located at the mass center of the HCO⁺ system. Considering the present collision energy region, the collision time is much shorter than the relaxation time of the target CO. Based on this argument, the CO distance is always fixed at the equilibrium geometry of the ground state of CO ($2.13222a_0$) during the calculation. In the present *ab initio* calculations for the H⁺/CO system, we use Dunning's cc-pVTZ basis sets for H, C, and O atoms [14]. The potential curves of the singlet states are obtained by the multireference single- and double-excitation configuration-interaction (MRD-CI) method [15], with configuration selection and energy extrapolation using the Table I algorithm [16]. In the CI calculations the two lowest molecular orbitals (MOs) are always kept doubly occupied, whereas the two highest ones are discarded. A small selection threshold [15] of 0.32×10^{-6} hartree has been used in the present treatment. More details of the present MRD-CI calculations can be found in Table I. The radial coupling matrix elements are obtained using calculated MRD-CI wave functions by a finite-difference method [17] with an increment of $0.0002a_0$, and the rotational coupling matrix elements are determined by a standard procedure [5].

B. Scattering dynamics

Scattering dynamics is studied on the basis of the fully quantum-mechanical formulation of a molecular-orbital expansion method in which dynamical transitions are driven by nonadiabatic couplings. The total scattering wave function is described in an adiabatic representation as an expansion in products of electronic and nuclear wave functions and the electron translation factor. Substitution of the total scattering wave function into the stationary Schrödinger equation yields coupled, second-order differential equations for the nuclear wave function $X^a(R)$. It is computationally convenient to solve the coupled equations in a diabatic representation [18]. The transformation from the adiabatic to the diabatic representation can be readily achieved through a unitary transformation matrix $C(R)$. In this representation the nuclear wave function for the heavy particles is related to $X^d(R) = C^{-1}X^a(R)$, and the diabatic potential matrix is $V^d = C^{-1}V^aC$, where V^a is the adiabatic potential matrix. The resulting coupled equations for $X^d(R)$ are given in matrix form as

$$\left[\frac{1}{2\mu} \nabla_R^2 I - V^d(R) + EI \right] X^d(R) = 0, \quad (2a)$$

and

$$E = k^2/(2\mu), \quad (2b)$$

where k is the momentum of the projectile, μ is the reduced mass of the system, I is the identity matrix, and V^d is the diabatic matrix. The coupled equation (2) is solved numerically to obtain the scattering S^l matrix for each partial wave l . The differential cross section is then obtained from the standard formula

$$\frac{d\sigma(\theta)}{d\Omega} = \frac{1}{4k^2} \left[\sum_l (2l+1) \{ \delta_{if} - S_{if}^l \} P_l(\cos\theta) \right]^2, \quad (3)$$

where S_{if}^l is the scattering S matrix element for partial wave l , and θ is the scattering angle in center-of-mass coordinates. Integration over all angles gives the total cross section. The limitation of this approach comes solely from our computational capability. As the collision energy increases to a few keV/ u region, the number of partial waves needed in the calculation exceeds a few thousand, which may make the numerical computation excessive.

Singlet states included in the dynamical calculations are as follows: for case I, the initial channel [$\text{H}^+ + \text{CO}(X^1\Sigma^+)$], $1^1A'$, electron-capture channel [$\text{H} + \text{CO}^+(X^2\Sigma^+)$], $2^1A'$, and electron-capture and excitation channel [$\text{H} + \text{CO}^{+*}(A^2\Pi)$], $1^1A''$, $3^1A'$. For both cases II and III, the initial channel [$\text{H}^+ + \text{CO}(X^1\Sigma^+)$], $1^1\Sigma^+$, electron-capture channel [$\text{H} + \text{CO}^+(X^2\Sigma^+)$], $2^1\Sigma^+$, and electron-capture and excitation channel [$\text{H} + \text{CO}^{+*}(A^2\Pi)$], $1^1\Pi$. The correspondence of the singlet states and their asymptotic limits are listed in Table II.

For some systems, differential cross sections and, sometimes, total cross sections display oscillatory structures as functions of collision energy or scattering angle. A semiclas-

TABLE II. The singlet states and the corresponding asymptotical limits of HCO^+ for three cases studied.

Asymptote	State (Cs) (Case I)	State (C_{∞}) (Cases II and III)
$\text{H}^+ + \text{CO}(X^1\Sigma^+)$	$1^1A'$	$X^1\Sigma^+$
$\text{H} + \text{CO}^+(X^2\Sigma^+)$	$2^1A'$	$2^1\Sigma^+$
$\text{H} + \text{CO}^+(^2\Pi)$	$3^1A', 1^1A''$	$1^1\Pi$

sical analysis for these structures would be sound and would improve the understanding of the underlying physics [18]. To discuss the scattering pattern, the deflection function $\Theta_J(L, E)$ must be determined for each trajectory and potential region J . This function is expressed as

$$\Theta_J(L, E) = \pi - 2b \int_{R_t}^{\infty} \left(1 - \frac{V(R)}{E} - \frac{b^2}{R^2} \right)^{-1/2} \frac{dR}{R^2}, \quad (4)$$

where b is the impact parameter and R_t is the inner zero (turning point) of the integrand. The parameter b relates to the orbital angular momentum L as

$$L^2 = 2\mu[E - V(\infty)]b^2, \quad (5)$$

where the classical quantity is connected to that of quantum mechanics. We have carried out the semiclassical analysis to identify the origin of oscillations in the differential cross sections shown below.

III. RESULTS

A. Adiabatic potentials and corresponding couplings

The adiabatic potentials for three different orientations are shown in Figs. 2(a)–2(c) for cases I–III, respectively, for all singlet states included in the scattering calculations. (See the schematic diagram of the initial molecular configuration as illustrated in Fig. 1.) Note that R is the distance between H^+ and the center of mass of the CO molecule.

In case I (H^+ approaches CO perpendicularly), the $1^1A'$ state corresponds to the initial H^+/CO channel whereas all the remaining states correspond to H/CO^+ charge transfer channels. It should be noted that the structures seen in $1^1A''$ and $3^1A'$ at $R = 2.5a_0$ and $3.3a_0$, respectively, are due to avoided crossings with high-lying states, and they are expected to become important only for higher energy collision dynamics. In both collinear cases (cases II and III), the $1^1\Sigma^+$ state corresponds to the initial H^+/CO channel whereas the remaining states belong to electron-capture channels. The $1^1\Pi$ states in case II and case III have avoided crossings with the high-lying $2^1\Pi$ state at about $R = 4.0a_0$ and $3.5a_0$, respectively, and again, these crossings may become important in the higher-energy regime. The $2^1\Sigma^+$ state also has an avoided crossing with higher $1^1\Sigma^+$ states in case II, whereas for case III it does not, at least for distances larger than $2a_0$. The curve crossing between the $2^1\Sigma^+$ and $1^1\Pi$ states for cases II and III is expected to play an important role in the flux redistribution between two electron-capture channels, and hence, explicit inclusion of

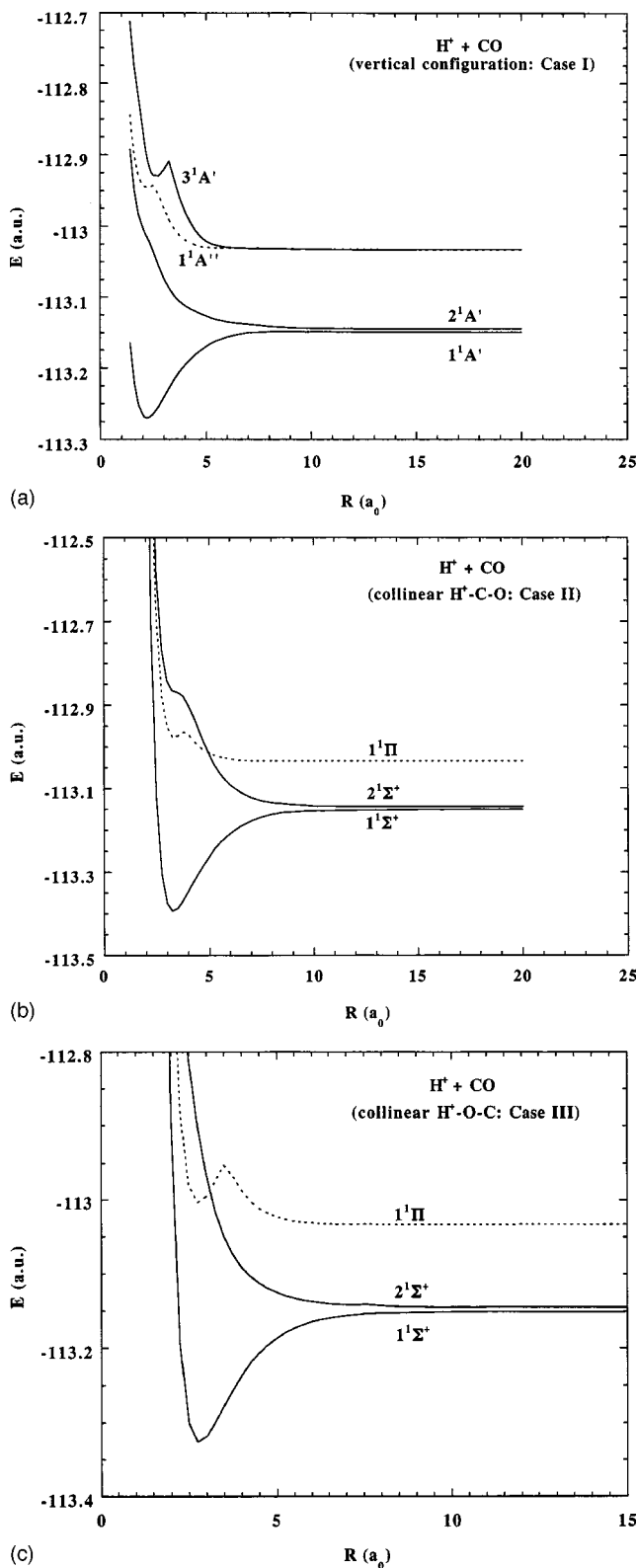


FIG. 2. Adiabatic potentials for (a) case I, (b) case II, and (c) case III.

the $1^1\Pi$ state is essential for accurate determination of partial cross sections. The calculated energy differences between the first H/CO^+ channel and the initial channel at $R = 20a_0$ are 0.14, 0.18, and 0.16 eV, for cases I–III, respec-

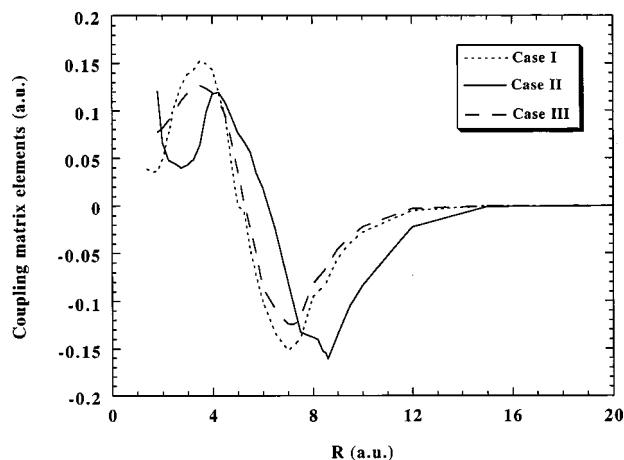


FIG. 3. Representative radial coupling matrix elements between the initial and the first electron-capture channels for three molecular configurations.

tively. Of course, at the asymptotic limit of $R = \infty$, these asymptotic energy differences should become the same for all three cases. The present asymptotic energy differences are somewhat better than those previously reported [19], while the high quality basis sets and a CI treatment are used in the present calculation. The experimental ionization potential of the CO molecule is 14.0 eV [20], and the present calculated value is 13.8 eV, which is within an accuracy of 2%. Therefore, we consider the present level of precision to be sufficient. Those between the second H/CO^+ channel and the initial channel are 3.18, 3.18, and 3.20 eV for cases I–III, respectively, which are found to be in good agreement with experiment. Note that for all three cases, the initial and first electron-capture channels show a typical Demkov-type coupling scheme [18].

Dominant radial coupling matrix elements between the initial and first electron-capture channels are plotted in Fig. 3 for all three configurations. This radial coupling between the initial and first electron-capture channels is the most important for the flux to exit to the upper levels. Generally, all three couplings show some similarities in both shape and magnitude, that is, a small hump near $R = 3.5-4a_0$, and a larger peak around $7-8a_0$. Depending on the molecular configuration, the position of the second peak is found to shift to larger R values. For example, for the case in which the proton approaches the C atom in the collinear configuration (case II), the peak position is found to be farther out at $R = 8.6a_0$, while for the cases which the proton approaches the O atom and the perpendicular approach, the location of the peak is nearly the same at around $7a_0$. These are reflections of the near-avoided crossings of the relevant potential curves. Also, the magnitude of the coupling varies slightly from one configuration to another. The small hump seen in the coupling below $4a_0$ plays a secondary role in the collision dynamics, as the dominant part is the major peak at around $6-8a_0$. It is interesting to examine how scattering dynamics are sensitive to these small changes in the couplings.

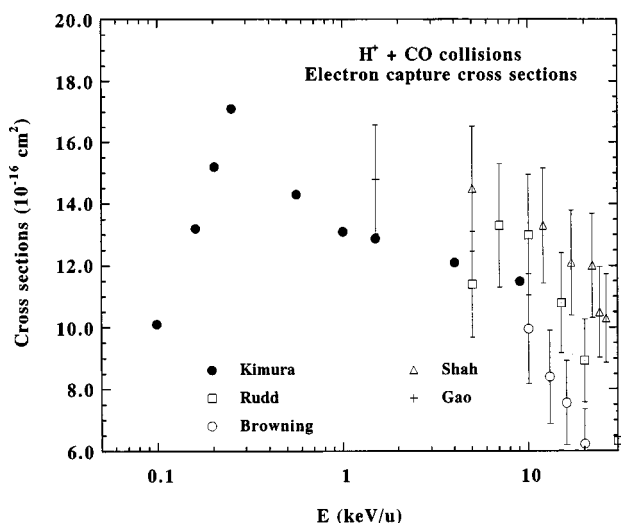


FIG. 4. Total electron-capture cross sections. ●, the present theory; □, Rudd *et al.* [11]; ○, Shah and Gilbody [12]; △, Browning and Gilbody [10]; +, Gao *et al.* [13].

B. Total cross sections

Total electron-capture cross sections averaged over the three molecular orientations, calculated within the quantum-mechanical molecular representation, are shown in Fig. 4. Three different types of the averaging procedure were considered in order to examine the procedure: (i) to sum over the scattering amplitudes and then to take the absolute square of them, (ii) to take the mean of the probability, and (iii) to integrate three total orientation-dependent cross sections over the orientation angle. The total cross sections determined with the three averaging procedures agree to within a few percent. As a consequence, the results reported below were obtained with procedure (i). Included in the figure are earlier experimental results by Browning and Gilbody [10], Rudd *et al.* [11], Shah and Gilbody [12], and Gao *et al.* [13]. Generally, the overall agreement with the present results and the four measurements is found to be very good. The maximum of the cross section is found to occur around 250 eV/u with a value of $1.71 \times 10^{-15} \text{ cm}^2$. The electron-capture cross section is found to decrease slowly for higher energies, and is consistent with all of the measurements. At 1.5 keV/u, our result reaches a value of $1.3 \times 10^{-15} \text{ cm}^2$, which compares favorably with that of Gao *et al.* who reported the value of $1.48 \times 10^{-15} \text{ cm}^2$. Shah and Gilbody reported the slightly smaller cross section with $1.0 \times 10^{-15} \text{ cm}^2$ at 10 keV/u, but the present result lies well within their error bars. In their measurement Browning and Gilbody found that CO^+ -ion formation is dominant for energies less than 10 keV/u. However, gradually, C^+ - and O^+ -ion formations increase with increasing collision energy. The present calculation has employed the fixed-nuclei approximation, which does not allow for the change of the C-O internuclear distance during the collision. Hence, information on the fragmentation is limited in the present investigation. However, based on the behavior of adiabatic potential curves for CO and CO^+ , we will make some inferences in regards to fragmentation below.

In the present calculation, the orientation for which the proton approaches the C atom in the collinear configuration (case II) is found to give the largest electron-capture cross section among the three configurations. The second largest contribution comes from case I, while case III is only the secondary effect. This is because the case I coupling peak is located at the largest internuclear distance among the three cases where the energy defect between the two channels becomes much smaller, and hence, they couple more effectively, making this case more ideal for electron capture. Furthermore, electron capture to the $[\text{H}+\text{CO}^+(X^2\Sigma^+)]$ channel is dominant for all energies studied, which is obvious from the energy defect between the relevant adiabatic potentials. Electron capture to the $[\text{H}+\text{CO}^+(^2\Pi)]$ channel is very weak in all three configurations, and in particular, at the lower end of the energy range their magnitudes are less than 10^{-18} cm^2 . They become comparable, however, with capture through the $[\text{H}+\text{CO}^+(X^2\Sigma^+)]$ channel at the highest energy in the present study. This finding is also obvious from the behavior of the adiabatic potentials and the endoergic nature of the reaction. As stated, even in the total cross section, the steric effect is remarkably conspicuous at 10 keV/u, although it begins to diminish at much higher collision energy.

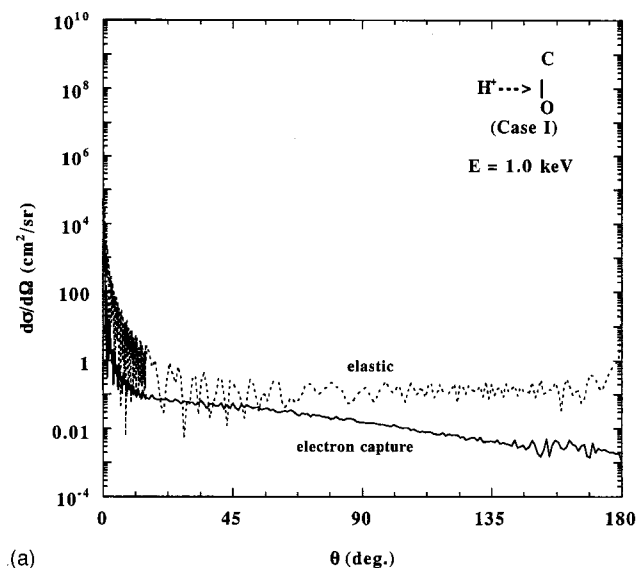
C. Differential cross sections (DCS's)

1. Theoretical results

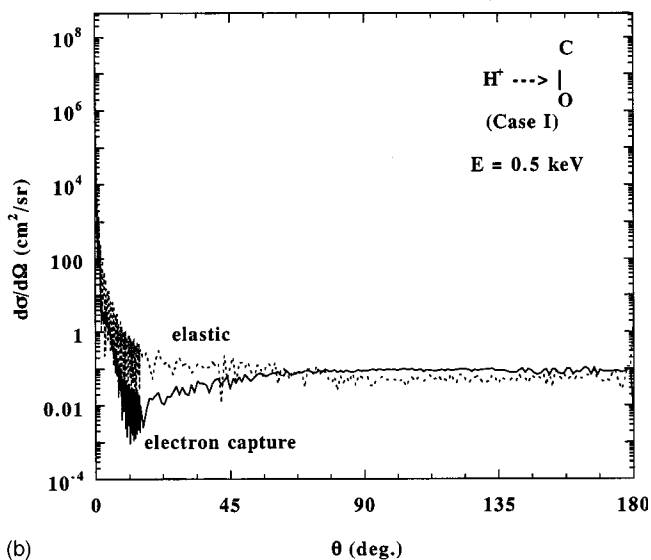
DCS's for elastic and electron-capture processes at 0.5 and 1 keV/u are shown in Figs. 5(a) and 5(b), 6(a) and 6(b), and 7(a) and 7(b) for cases I, II, and III, respectively. We first discuss the details for each case separately, and then summarize the similarities and differences of the three cases.

Case I. Both elastic and electron-capture DCS's at all energies show strongly oscillatory characters. This is particularly so below 20° , and these strong and rapid oscillations are due to the interference arising from the anisotropy of the charge distribution of the CO molecule. At 0.5 keV/u, above 40° or so, the magnitude of elastic and electron capture DCS's are comparable, while as the collision energy increases to 1.0 keV/u, the magnitude of elastic DCS becomes much larger by a few orders of magnitude in the small angle region. Since only a small contribution to the total cross section comes from angles greater than or equal to a few 10° , the elastic process is still dominant in the total cross section. Small but conspicuous oscillatory structures remain as the collision energy increases.

Case II. Electron-capture DCS's show sharp dips at just below 40° and 130° at 0.5 keV/u, and at around 90° for 1 keV/u. Based on the semiclassical analysis, these dips are identified due to the rainbow scattering. Except for these dips, the general shape of the DCS's is rather flat beyond the scattering angle of around 20° for both energies. Elastic DCS's show mild wiggles at 0.5 keV/u, but they begin to diminish at 1 keV/u. The magnitude for the elastic DCS is slightly larger than that of electron capture beyond 20° . Below this scattering angle, the magnitude of the elastic DCS dominates. Particularly below 1° , the elastic DCS's are larger by one or two orders of magnitude over those of elec-



(a)



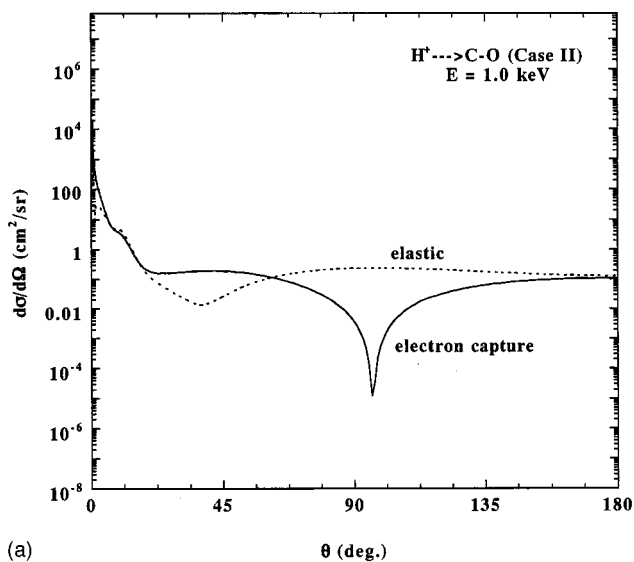
(b)

FIG. 5. Differential cross sections for case I at (a) 1.0 keV/u and (b) 0.5 keV/u. Both elastic and electron capture DCS's are shown.

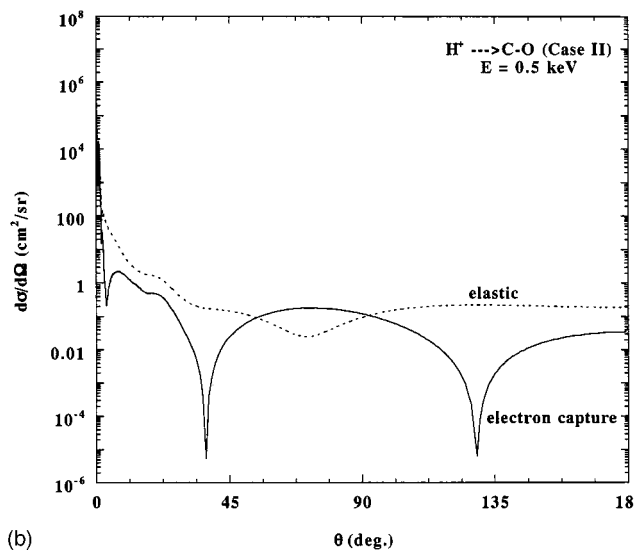
tron capture. In fact this is the region that gives the dominant contribution to the total cross section when integrated over the angle.

Case III. Electron-capture DCS's near 0.5 and 1 keV/u show a sharp dip due to the rainbow scattering at 40° and 60°, respectively, which shifts from 40° toward 60° as the collision energy decreases. This observation is consistent with the semiclassical analysis. Except for this dip, the shapes of the DCS's near at 0.5 and 1 keV/u are fairly constant beyond 20°. Elastic DCS's are also nearly flat beyond 20° and no strong structure is seen. Below 20°, however, some few oscillatory structures are found in both elastic and capture processes, and at near 0°, both reach a magnitude of about 10^7 cm²/sr. The difference in the DCS's at near 0° and the flat region from 20° to 170° is more than 10^7 cm²/sr, and hence, most of the contribution to the total cross section comes from the region below the 12° region.

For all three molecular configurations, a large magnitude of the DCS's of nearly 10^6 – 10^7 cm²/sr arise only from the



(a)



(b)

FIG. 6. Differential cross sections for case II at (a) 1.0 keV/u and (b) 0.5 keV/u. Both elastic and electron capture DCS's are shown.

narrow region of the scattering angle below 10°–12°. For larger angles, all DCS's drop very sharply by orders of magnitude reaching 10^{-2} cm²/sr. Beyond around 20°, both elastic and electron-capture DCS's, regardless of whether they show small oscillations and dips, become flat in magnitude. These features are common in all collision energies studied generally, although as the collision energy decreases, somewhat more pronounced differences in each DCS begin to emerge, suggesting a more marked steric effect. It is also worthwhile noting that the position of the rainbow dip for the cases II and III are located at 90° and 60°, respectively, in electron-capture DCS's at 1 keV/u. This difference clearly manifests itself from the steric effect as discussed below.

2. Comparison with experimental DCS's

There is only one experimental attempt to measure the differential cross section for this collision system [13] in the

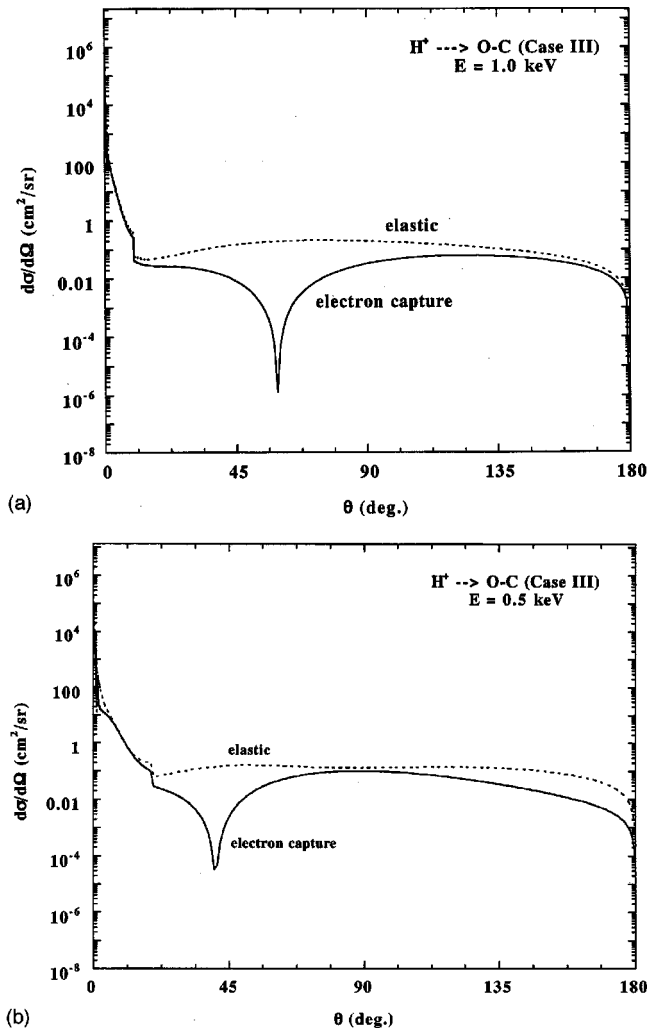


FIG. 7. Differential cross sections for case III at (a) 1.0 keV/ u and (b) 0.5 keV/ u . Both elastic and electron capture DCS's are shown.

scattering angle range from 0.02° to 1.0° and at 1.5 keV/ u . They claimed that their angular resolution is better than 0.008°. The present theoretical results along with the experimental data are shown in Fig. 8. The present results averaged over the molecular configuration at 1.5 keV/ u are found to be in good agreement with the experimental result over the entire range of the scattering angles. The two visible structures in the DCS's are one maximum at the angle of 0.08°, and another peak at 0.2°, both of which are well reproduced by the theory, although the theoretical positions shift slightly towards higher angles. Two sharp dips at 0.05° and 0.15° are also reproduced by the theory reasonably well. The theoretical magnitude of the DCS is in reasonable accord with the measurement. The origin of these two structures are a combination of the interference between elastic and electron-capture channels and between different molecular configurations. The theoretical DCS above 0.2° displays regular oscillatory structures, while the experimental results decrease rather monotonically. The discrepancy between the two may be, in part, due to an insufficient experimental resolution for detecting these oscillations. This good agreement at small

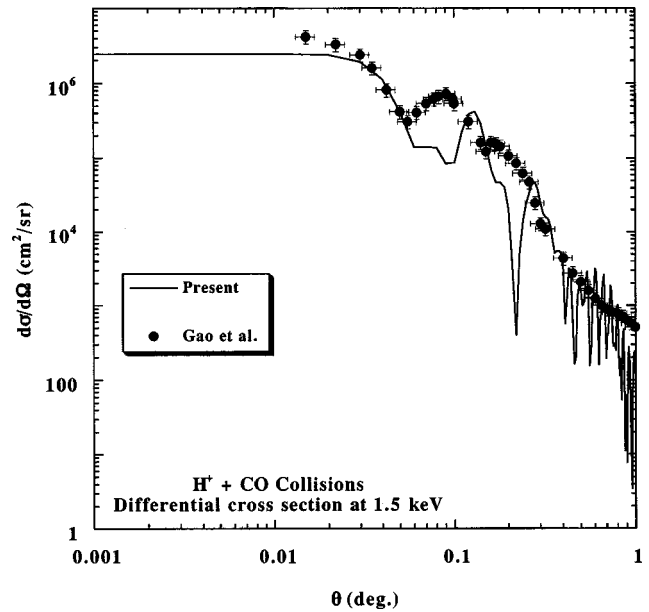


FIG. 8. DCS's averaged over the molecular configuration as a function of the scattering angle from 0.001° to 1° at the collision energy of 1.5 keV/ u . Solid circles are the experimental data by Gao *et al.* [13].

angles confirms that our adiabatic potentials and coupling matrix elements employed are of reasonable precision at least for the asymptotic region, which controls the small angle scattering. However, the agreement appears to become less satisfactory as the scattering angle increases although general agreement is still good considering the difficulty in the experiment and theory. The large angle scattering corresponds to small impact-parameter collisions, and hence molecular states lying at higher levels, which we entirely neglected in the present dynamical calculation, may begin to participate in the dynamics.

D. The steric effect

It is apparent from the discussion on the DCS's above that electron capture is very sensitive to the molecular orientation, i.e., the steric effect, and we take a close look at this feature. In Fig. 9 we present the scattering S -matrix elements for all three molecular configurations at the collision energy of 0.5 keV/ u , and some features can be summarized: (i) the magnitude for case III is the smallest of all, while that for case II is the largest, (ii) the number of oscillations is different for the three cases, and (iii) for case II, the last tail of the S -matrix element stretches out for the largest l value. All these characteristics are the reflection of those of the dominant radial coupling matrix elements seen in Fig. 2, coupled with the features of the adiabatic potentials, and are clear manifestations of the steric effect due to the molecular charge distribution. In fact there is no obvious similarity in the S -matrix elements and hence, in the DCS's among the three configurations, the strong steric effect is demonstrated. As the collision energy increases to 10 keV/ u , the highest energy we studied, this feature of the steric effect is found to still persist. From the present study, it may be possible that

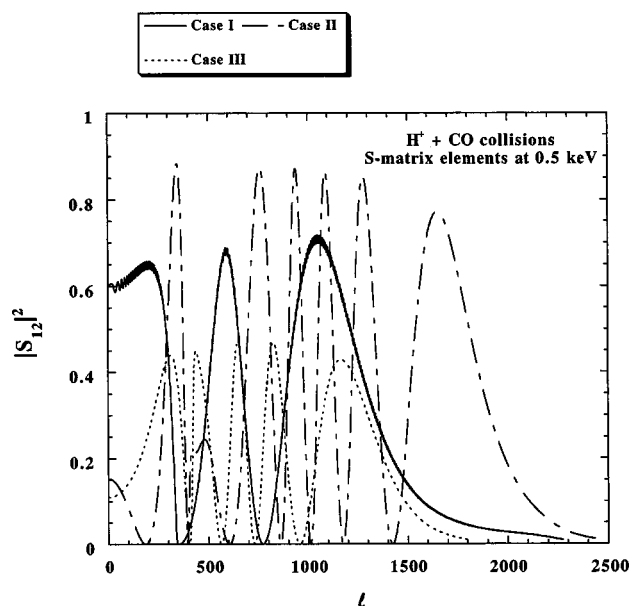


FIG. 9. Scattering S -matrix elements for three molecular configurations at 0.5 keV/ u .

the geometrical structure of the target molecule can be analyzed based on the perturbative procedure similar to an electron scattering study [21].

E. Fragmentation

For the H^+/CO system, the energy difference between the initial channel [$H^+ + \text{CO}(X^1\Sigma^+)$] and the charge-transfer channel [$H + \text{CO}^+(X^2\Sigma^+)$] is very small (less than 0.5 eV), and the values of the coupling elements between these two channels are sizable, as seen in Fig. 3. Thus, the charge transfer between the initial and the [$H + \text{CO}^+(X^2\Sigma^+)$] channels is extremely effective. The final products of the charge-transfer process depend on the energy transferred to CO^+ in the collision process. The lowest CO^+ state is deeply bound, with a binding energy of about 8.3 eV [20] and has a nearly identical equilibrium internuclear distance to that of the ground state of CO. Above this state, there exist several bound and repulsive states asymptotically corresponding to $C^+(^2P^0)/O(^3P)$ and $C^+(^2P^0)/O(^1D)$. The energy defect between the first ion-pair $C^+(^2P^0)/O(^3P)$ state and next higher $C^+(^2P^0)/O(^1D)$ state is only 1.97 eV [22]. At still higher energy, there are states asymptotically corresponding to $C(^3P)$ and $O^+(^4S^0)$, which is 0.4 eV above $C^+(^2P^0)/O(^1D)$ [23]. Therefore, in view of the Franck-Condon principle, it seems likely that most of the CO^+ ions produced in the charge-transfer process will be in the low-lying bound states of CO^+ and be quite stable. When the amount of the energy transferred to CO^+ is large, the low-

lying repulsive states could be reached, leading to the generation of C^+ ions. As more energy transferred to CO^+ becomes available, O^+ ions could also be produced since it is then possible to reach still higher repulsive states (more repulsive states leading to C^+/O could also be populated). According to Shah and Gilbody [12], at 13 keV/ u , the dominant products observed in their experiment are CO^+ molecular ions (84% CO^+). The yield of O^+ ions is smaller than that of C^+ ions by a factor of two. At higher energy (98 keV/ u), the amount of CO^+ decreases to 75%, and the ratio of C^+ to O^+ yields increases to three.

IV. CONCLUSIONS

We have carried out theoretical investigations of electron capture in $H^+ + \text{CO}$ collisions in the collision energy from 0.1 to 10 keV/ u based on the fully quantum mechanical molecular representations. Three molecular configurations are specifically considered: (i) the proton approaches the center of mass of the CO molecule in the perpendicular configuration (case I), (ii) the proton approaches the C atom in the collinear configuration (case II), and (iii) the proton approaches the O atom in the collinear configuration (case III). Cases I and III are found to be dominant contributors to electron capture, while case II is found to be secondary. The present total capture cross section, obtained by averaging over the molecular configurations, is in good agreement with all experimental data available in magnitude as well as energy dependence. The present DCS's are also in good agreement with the experiment by Gao *et al.* [13] for scattering angle from 0.01° to 1° at 1.5 keV/ u , in which the theory can reproduce the oscillatory structures quite well. The steric effect is found to persist rather significantly in all energies studied as described in detail. The present cross-section data are considered to be useful for various applications.

ACKNOWLEDGMENTS

The work was supported in part by the grant-in-aid, the Ministry of Education through Yamaguchi University (M.K.), and by the Deutsche Forschungsgemeinschaft in the form of a Forschergruppe and Grant No. Bu450/7 and by the National Science Foundation through a grant to the Institute for Theoretical Atomic and Molecular Physics at Harvard University and Smithsonian Astrophysical Observatory (M.K., J.P.G., and R.J.B.). The financial support of the Fonds der Chemischen Industrie is also hereby gratefully acknowledged. Finally M.K. acknowledges the support from the Deutsche Akademische Austauschdienst (DAAD) through Universität Wuppertal during the time when much of this study was performed. P.C.S. acknowledges support from a grant from NASA Ultraviolet, Visible, and Gravitational Program.

- [1] H. Nakamura, *Adv. Chem. Phys.* **LXXXII**, 243 (1992).
 [2] F. A. Gianturco and F. Schneider, *Adv. Chem. Phys.* **LXXXII**, 135 (1992).
 [3] H. J. Loesch, *Annu. Rev. Phys. Chem.* **46**, 555 (1995).

- [4] K. Kuwata and T. Kasai, *Adv. Ser. Phys. Chem.* **6**, 844 (1995).
 [5] M. Kimura, Y. Li, G. Hirsch, and R. J. Buenker, *Phys. Rev. A* **52**, 1196 (1995).
 [6] M. Kimura, Y. Li, G. Hirsch, and R. J. Buenker, *Phys. Rev. A*

- 54**, 5019 (1996).
- [7] W.-H. Ip, *Astrophys. J.* **343**, 946 (1989).
- [8] P. Bochslers, *Phys. Scr.* **T18**, 55 (1987).
- [9] M. J. Mumma *et al.*, *Science* **272**, 1310 (1996).
- [10] R. Browning and H. B. Gilbody, *J. Phys. B* **1**, 1149 (1968).
- [11] M. E. Rudd, R. D. DuBois, L. H. Toburen, C. A. Ratcliffe, and T. V. Goffe, *Phys. Rev. A* **28**, 3244 (1983).
- [12] M. B. Shah and H. B. Gilbody, *J. Phys. B* **23**, 1491 (1990).
- [13] R. S. Gao, L. K. Johnson, C. L. Hakes, K. A. Smith, and R. F. Stebbings, *Phys. Rev. A* **41**, 5929 (1990).
- [14] T. H. Dunning, Jr., *J. Chem. Phys.* **90**, 1007 (1989).
- [15] R. J. Buenker and S. D. Peyerimhoff, *Theor. Chim. Acta* **35**, 33 (1974); **39**, 217 (1975); R. J. Buenker, *Int. J. Quantum Chem.* **29**, 435 (1986); S. Krebs and R. J. Buenker, *J. Chem. Phys.* **103**, 5613 (1995).
- [16] R. J. Buenker, in *Proceedings of the Workshop on Quantum Chemistry and Molecular Physics, Wollongong, Australia*, edited by P. G. Burton (University Press, Wollongong, 1980); in *Studies in Physical and Theoretical Chemistry*, edited by R. Carbo, *Current Aspects of Quantum Chemistry Vol. 21* (Elsevier, Amsterdam, 1981), p. 17; R. J. Buenker and R. A. Phillips, *J. Mol. Struct.: THEOCHEM* **123**, 291 (1985).
- [17] G. Hirsch, P. J. Bruna, R. J. Buenker, and S. D. Peyerimhoff, *Chem. Phys.* **45**, 335 (1980).
- [18] M. Kimura and N. F. Lane, *Adv. At., Mol., Opt. Phys.* **26**, 79 (1989).
- [19] P. J. Bruna, S. D. Peyerimhoff, and R. J. Buenker, *Chem. Phys.* **10**, 323 (1975).
- [20] K. P. Huber and G. Herzberg, *Molecular Spectra and Molecular Structure, Constants of Diatomic Molecules Vol. 4* (Van Nostrand Reinhold, New York, 1979).
- [21] J. W. Liu and R. A. Bonham, *J. Mol. Struct.* **11**, 297 (1972).
- [22] H. Lavendy, J. M. Robbe, and J. P. Flament, *Chem. Phys. Lett.* **205**, 456 (1993).
- [23] C. E. Moore, *Atomic Energy Levels*, Natl. Bur. Stand. (U.S.) Circ. No. 467 (U.S. GPO, Washington, D. C., 1949), Vol. 1.